Carnegie Observatories Astrophysics Series, Vol. 2:
Measuring and Modeling the Universe, 2004
ed. W. L. Freedman (Cambridge: Cambridge Univ. Press)

LIGO at the Threshold of Science Operations

ALBERT LAZZARINI
LIGO Laboratory, California Institute of Technology

Abstract

LIGO held its first science run during the two and one-half week period from 23 August to 9 September 2002. The strain sensitivity of the interferometers during this observational period was $h(f) \approx 10^{-20}\,\mathrm{Hz}^{-\frac{1}{2}}$ at $f \approx 300\,\mathrm{Hz}$. The useful instrumental bandwidth spanned the decade $100\,\mathrm{Hz} \lesssim \mathrm{f} \lesssim 1000\,\mathrm{Hz}$. During the 17-day period, the three km-scale LIGO interferometers (2 and 4 km in WA and 4 km in LA) and the 600 m GEO interferometer (outside Hanover, Germany) operated as a network of detectors for part of the time.

The LIGO Scientific Collaboration is presently analyzing the first data run (S1) for a number of classes of sources of gravitational radiation. Working groups within the collaboration are performing searches for signatures coming from four classes of gravitational wave (GW) sources. These include: (1) continuous wave sources (GW counterparts to electromagnetic pulsars), (2) burst or transient sources, such as GW emission from supernovae, (3) inspiral and coalescence of compact binary systems, and (4) a stochastic GW background. The emphasis in this first science run will be to develop the analysis techniques and software pipelines that will be used to analyze data continuously during periods of extended observation in future science runs. At the same time, the S1 data quality are such that it should be possible to provide improved *direct observational* limits on gravitational radiation with these fundamentally new instruments.

1.1 Introduction

In the last few years a number of new gravitational wave (GW) detectors, using long-baseline laser interferometry, have begun to enter into operation. These include the Laser Interferometer Gravitational Wave Observatory (LIGO; Abramovici et al. 1992; Barish & Weiss 1999) detectors located in Hanford, WA and Livingston, LA, built by a Caltech-MIT collaboration, the GEO-600 detector near Hanover, Germany, built by an British-German collaboration (Danzmann et al. 1995), the VIRGO detector near Pisa, Italy, built by an Italian-French collaboration (Caron et al. 1995), and the Japanese TAMA-300 detector in Tokyo (Tsubono 1995). While none of these instruments is yet performing at its design sensitivity, many have begun making dedicated data collecting runs and performing GW search analyses on the data.

In particular, from 23 August to 9 September 2002, the LIGO Hanford and LIGO Liv-

Table 1.1. *Operational Duty Cycles of Different Coincidence Modes during S1*

	Locked Time (Hr)	Duty Cycle (%)
	Single	
H1 (4 km)	235	57.6
H2 (2 km)	298	73.1
L1(4 km)	170	41.7
	Double Coincidence	
H1+L1	116	28.4
H2+L1	131	32.1
H1+H2	188	46.1
	Triple Coincidence	
H1+H2 +L1	95.7	23.4

ingston Observatories (LHO* and LLO†) took coincident science data (referred to as S1). The LHO site contains two, identically oriented interferometers, one having 4 km long measurement arms (referred to as H1), and the other having 2 km long arms (H2); the LLO site contains a single, 4 km long interferometer (L1). GEO also took data in coincidence with the LIGO detectors during that time, although with significantly poorer sensitivity.

The LIGO Scientific Collaboration* is presently analyzing the first data run (S1) for a number of classes of sources of gravitational radiation. Working groups within the collaboration are conducting searches for signatures coming from four classes of GW sources. These include: (1) continuous wave sources, such as periodic sources [GW counterparts to electromagnetic (EM) pulsars], (2) burst or transient sources, such as GW emissions from supernovae or other transient events, (3) inspiral and coalescence of compact binary systems, (4) a stochastic GW background. The emphasis in this first science run will be develop the analysis techniques and software pipelines that will be used to analyze data continuously during periods of extended observation in future science runs. At the same time, the S1 data quality are such that it should be possible to provide improved *direct observational* limits on gravitational radiation with these fundamentally new instruments.

Figure 1.1 presents a composite graph showing the amplitude spectral densities for the three LIGO interferometers taken during the S1 run. The LA 4 km machine was the most sensitive, achieving strain sensitivities of $h(300\,\mathrm{Hz}) \approx 3 \times 10^{-21}\,\mathrm{Hz}^{-\frac{1}{2}}$. Table 1.1 presents the operational duty cycles for the different coincidence modes during S1. During S1, LIGO interferometers had better broad-band sensitivities than any prior GW detector. In addition, the number of machines operating simultaneously was unprecedented.

* http://www.ligo-wa.caltech.edu
† http://www.ligo-la.caltech.edu
* http://www.ligo.org

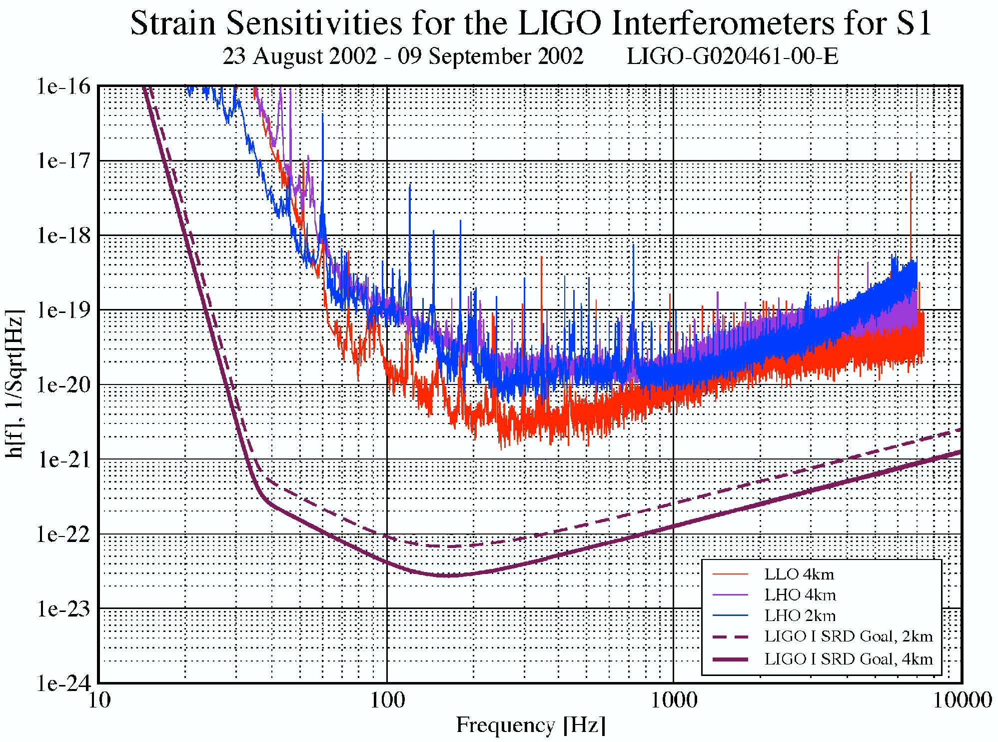

Fig. 1.1. Spectra of instrumental sensitivities for the three LIGO interferometers during the S1 science run. The solid curve corresponds to the design goal for the 4 km long interferometers in WA and LA. The dashed curve gives the goal for the shorter, 2 km long instrument in WA.

1.2 S1 Data Analysis Activities

At the time of this writing, the LIGO Scientific Collaboration is still processing the data, and it is not yet possible to publicize the results. The discussion below will concentrate on techniques being applied in the data analysis.

In all cases, data analysis pipelines have been set up to provide production capability to process data end-to-end. These pipelines also provide support for Monte Carlo simulations that are required to validate and to calibrate the search efficiencies. Figure 1.2 presents a block diagram schematic of the analysis flow for the burst event search. It is representative of a prototypical analysis pipeline.

Data streams from an interferometer are processed by a data analysis flow that generates candidate events. These events are subsequently analyzed for coincidence among as many interferometers as were operating at the epoch when the candidate event was produced. The GW (strain) channel is processed by *event trigger generator* filter(s) that perform optimal filtering of the strain channel using either template waveforms based on astrophysical source models or parameterizable waveforms (e.g., wavelets) that are correlated continuously against the interferometer output. When the event trigger exceeds a threshold deter-

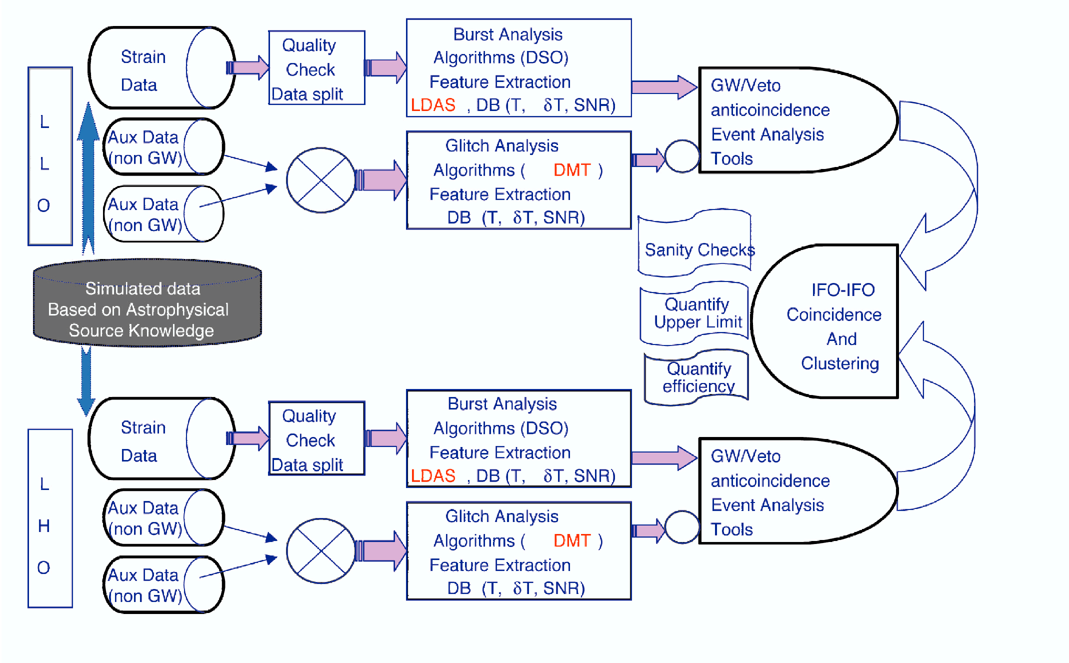

Fig. 1.2. The burst analysis pipeline as a prototypical analysis technique. Notation: DSO — a search algorithm library; LDAS — LIGO Data Analysis System environment; DB — relational database used to archive event metadata; DMT — data monitoring tool suite used to look at non-strain channel data in near real time; IFO — interferometer; LHO — LIGO Hanford Observatory; LLO — LIGO Livingston Observatory.

mined by Monte Carlo calibration of the pipeline, a putative event is identified for further post-processing downstream.

A variety of auxiliary channels are used to monitor instrumental and environmental characteristics at the same time the strain channel is analyzed. Transient or off-nominal behavior of these other channels is used to *veto* candidate events during epochs of detection when the instrument was not operating in its quiescent state. Candidates that survive these vetoes are then processed for coincidence among the several interferometers. Further, consistency checks are enforced to verify, for example, that the coincident events are consistent in all interferometers: comparable signal amplitude, duration, and frequency content are required of a coincidence for it to be considered a possible astrophysical event.

Interpretation of the results requires that models of source distributions, source strengths, and waveform characteristics be injected into the data stream using Monte Carlo techniques. In this way the detection efficiency can be determined for different classes of signals.

1.2.1 Classes of GW Sources

Different types of GW sources produce signals with specific signatures encoded in the waveforms. These signatures are exploited using digital signal processing techniques to identify candidate events. Figure 1.3 presents a simulated time-frequency map showing

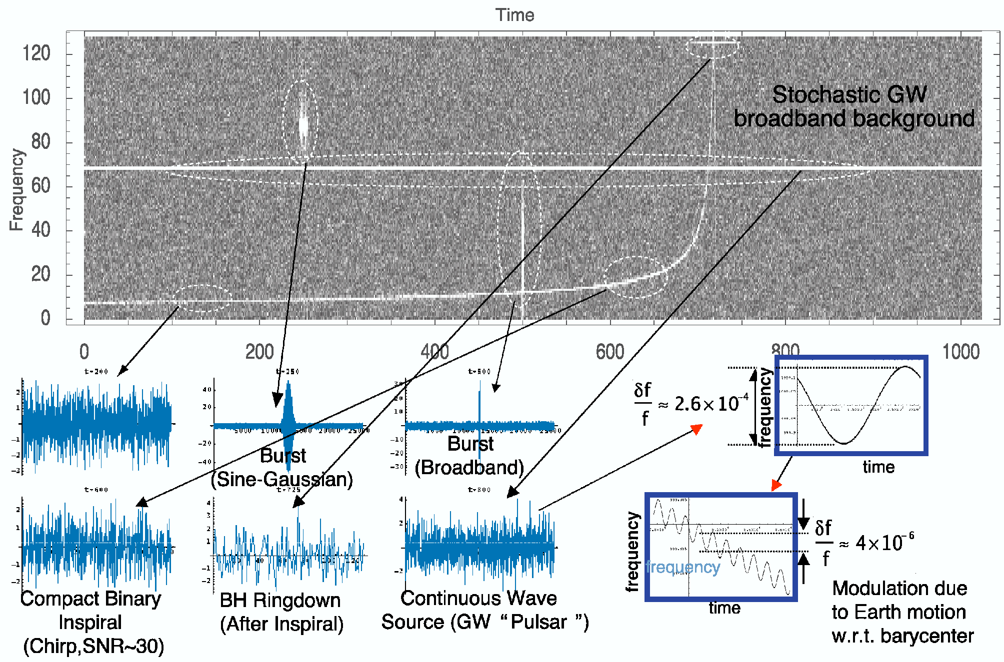

Fig. 1.3. Simulated time-frequency map showing the various classes of GW sources and their characteristic evolution in time. Inspirals produce chirps with a characteristic upswing in frequency. Periodic sources are expected to produce monochromatic signals with an impressed FM signature from the barycentric motion of the Earth. The daily rotation produces a $\sim 10^{-6}$ effect and the orbital motion produces a $\sim 10^{-4}$ effect. Bursts are expected to produce short-duration broad-band signals. The stochastic background is stationary, isotropic, and broad band. Optimal filters exploit the time-dependent evolution of signal phase (or frequency) to discriminate against background noise.

these signatures. Searches for the different source types are discussed in the following subsections.

1.2.1.1 Searches for Periodic Sources of GW

Periodic sources are narrow-band coherent signals that extend over the entire period of observation. For sufficiently long observations, the deterministic and well-characterized frequency modulations (FM) imposed by the barycentric motion of the Earth around the Sun can be exploited to verify the extraterrestrial nature of such a source. On the scale of the S1 run, only a portion of the yearly FM cycle is detectable, and the FM signatures correspond to monotonic drifts in signal frequency upon which is superimposed the daily modulations caused by Earth rotation.

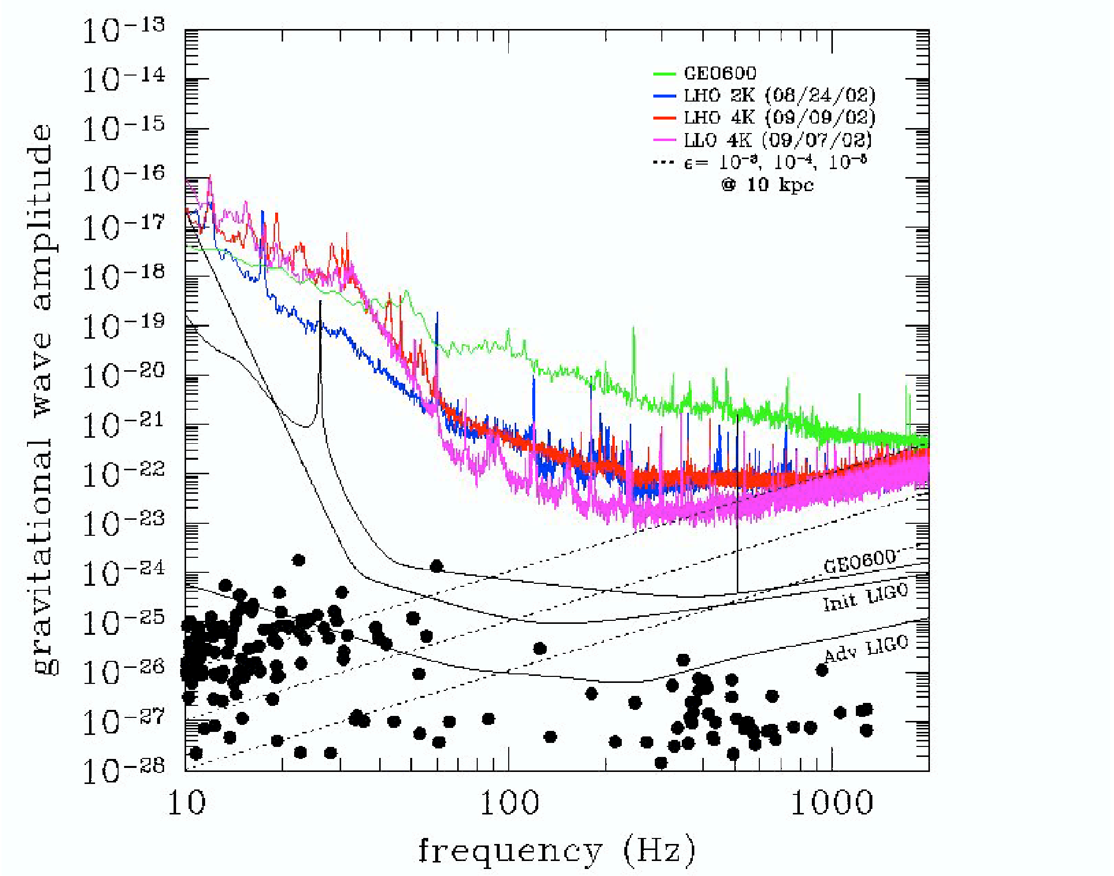

Fig. 1.4. Composite graph showing the S1 strain sensitivities of the four interferometers participating in the science run. The labeled smooth curves correspond to design sensitivities. Data and curves are scaled to show the critical amplitude, $h_c(f) \equiv 4.2\sqrt{S_h(f)/T_{\rm obs}}$ detectable with 99% confidence during the duration of S1, $T_{\rm obs} \approx 17\,$d. The individual dots correspond to known EM millisecond pulsars. The abscissa is *twice* the EM frequency. The ordinate corresponds the the signal that would be generated *if* observed spin-downs were attributable entirely to GW emission. This provides an astrophysical upper limit derived from energy conservation arguments. The dashed lines (from top to bottom) give the signal strength as a function of frequency for rotating compact stars with equatorial ellipticities of $\epsilon = 10^{-3}, 10^{-4}$, and 10^{-5} at a distance of 10 kpc, corresponding approximately to sources at the center of the Galaxy. (Figure courtesy of R. Depuis, Univ. of Glasgow/GEO.)

The first analyses of LIGO data will search for evidence of GW emission from specific sources with known EM counterparts. Figure 1.4 presents a "landscape" of sensitivities achieved during S1 and possible sources of GW associated with known EM counterparts. *Directed* or *targeted* searches looking at such sources will be employed to validate the analysis techniques and to set direct observational upper limits at progressively more interesting levels. Broad-band interferometers will allow simultaneous observation and parallel analysis of many sources—something not previously possible with resonant cryogenic bars. Previously

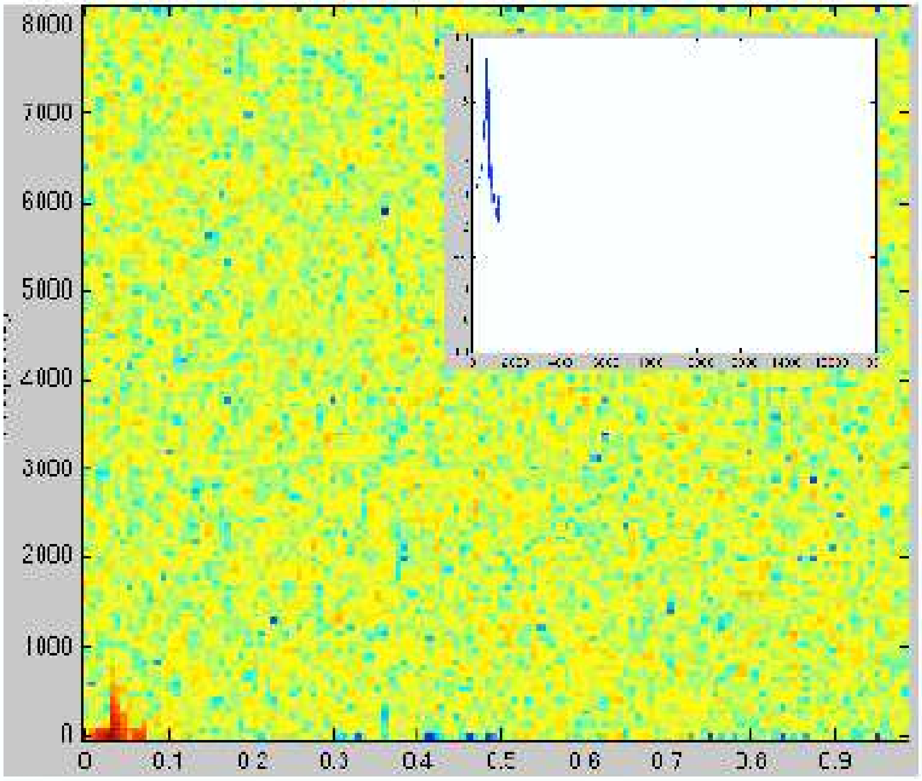

Fig. 1.5. Output of tfclusters for a time-frequency image of a Zwerger-Muller supernova waveform (at $\{t, f\} = \{0.05\text{s}, 0 \rightarrow 500\,\text{Hz}\}$).

published observational limits for periodic sources are $h_{max}(f = 1283.86\,\text{Hz}) \leq 3 \times 10^{-20}$ for PSR1939+2134 (Hough et al. 1983) using an interferometer, and $h_{max}(f = 921.35\,\text{Hz}) \leq 3 \times 10^{-24}$ for an untargeted search toward the center of the Galaxy at a frequency constrained by the resonant bar detector (Astone et al. 2002).

In the future the plan is to expand the searches to include other periodic sources, such as low-mass X-ray binaries (e.g., Sco-X1). In addition, a blind search technique is being developed to search for potential GW sources having no known EM counterparts. Such a search targets large portions of the sky and does a parametric search over intrinsic source characteristics (e.g., spin down rates) and extrinsic parameters, such as sky location and their effect on the signal FM characteristics (Brady et al. 1998; Brady & Creighton 2000). Examples of such sources include rapidly rotating, newly formed neutron stars (Andersson 1998; Friedman & Morsink 1998; Lindblom, Owen, & Morsink 1998; Andersson, Kokkotas, & Schutz 1999; Bildsten & Ushomirsky 2000; Jones 2001; Lindblom & Owen 2001; Arras et al. 2003).

Table 1.2. *Rate Estimates for Inspiral of NS/NS, NS/BH, and BH/BH Binaries*†

	NS/NS	NS/BH	BH/BH in Field	BH/BH in Clusters
$\mathcal{R}_{\rm gal}$ (yr^{-1})	10^{-6}–5×10^{-4}	$\lesssim 10^{-7}$–10^{-4}	$\lesssim 10^{-7}$–10^{-5}	$\sim 10^{-6}$–10^{-5}
$D_{\rm I}$ (Mpc)	20	43	100	100
$\mathcal{R}_{\rm I}$ (yr^{-1})	$3\times10^{-4}-0.3$	$\lesssim 4\times10^{-4}-0.6$	$\lesssim 4\times10^{-3}-0.6$	$\sim 0.04-0.6$
$D_{\rm WB}$ (Mpc)	300	650	$z=0.4$	$z=0.4$
$\mathcal{R}_{\rm WB}$ (yr^{-1})	$1-800$	$\lesssim 1-1500$	$\lesssim 30-4000$	$\sim 300-4000$

†Table adapted from Cutler & Thorne (2002); refer to this reference for the primary sources of these estimates. The table shows estimated rates $\mathcal{R}_{\rm gal}$ in the Galaxy (with masses $\sim 1.4M_\odot$ for NS and $\sim 10M_\odot$ for BH), the distances $\mathcal{D}_{\rm I}$ and $\mathcal{D}_{\rm WB}$ to which initial interferometers and advanced wide-band (WB) interferometers can detect them, and corresponding estimates of detection rates $\mathcal{R}_{\rm I}$ and $\mathcal{R}_{\rm WB}$. The third row, $\mathcal{R}_{\rm I}$, corresponds to the present generation of LIGO interferometers.

1.2.1.2 Searches for Burst Sources of GW

Burst sources have no deterministic phase or frequency evolution and thus template-based modeling of source properties is not applicable. Instead, techniques predicated on *novelty detection* are being developed. By novelty detection is meant a search algorithm that employs statistical methods to characterize the data stream over periods of time that are much longer than the expected duration on burst events, then to use these prior characteristics of the data to set thresholds looking for excess signal power on time scales of fractions of a second.

For the S1 run, two techniques have been developed. One approach searches in the time domain and detects the amplitude fluctuations of the signal on short time scales. The other approach utilizes time-frequency maps of the strain channel to look for clustering of contiguous pixels that exceed a predetermined threshold. The former approach implements an algorithm, termed *slope filter*, which looks for large changes of slope over short periods of time. The algorithm is a subset of a more general algorithm developed by the Orsay group (Pradier et al. 2001). The latter approach is being used in two similar implementations. The first of these, termed *excess power* (Anderson et al. 2000, 2001), tessellates the $t-ft-f$ plane into "postage-stamp" patches of constant $\Delta f\Delta t$ and looks for excess power fluctuations. The second algorithm, termed *tfclusters* (Sylvestre 2002), has a clustering algorithm that is able to identify and detect groups of contiguous pixels that have arbitrary shape. Both approaches have been shown capable of detecting excess power embedded in a noisy signal. Figure 1.5 depicts an image of the $t-f$ output of tfclusters for an injected Zerger-Müller (1997) supernova waveform. These same techniques are suitable for detecting black hole ringdowns.

A subgroup of the burst search team is also developing search methodologies for so-called *externally* triggered searches, whereby astrophysical triggers (e.g., gamma-ray burst events) can be used to localize in time searches for coincidences among multiple interferometers. By such techniques, it is possible to provide upper limits, in lieu of detection, of the amount of GW energy associated with externally triggered events seen by other detectors (Finn, Mohanty, & Romano 1999).

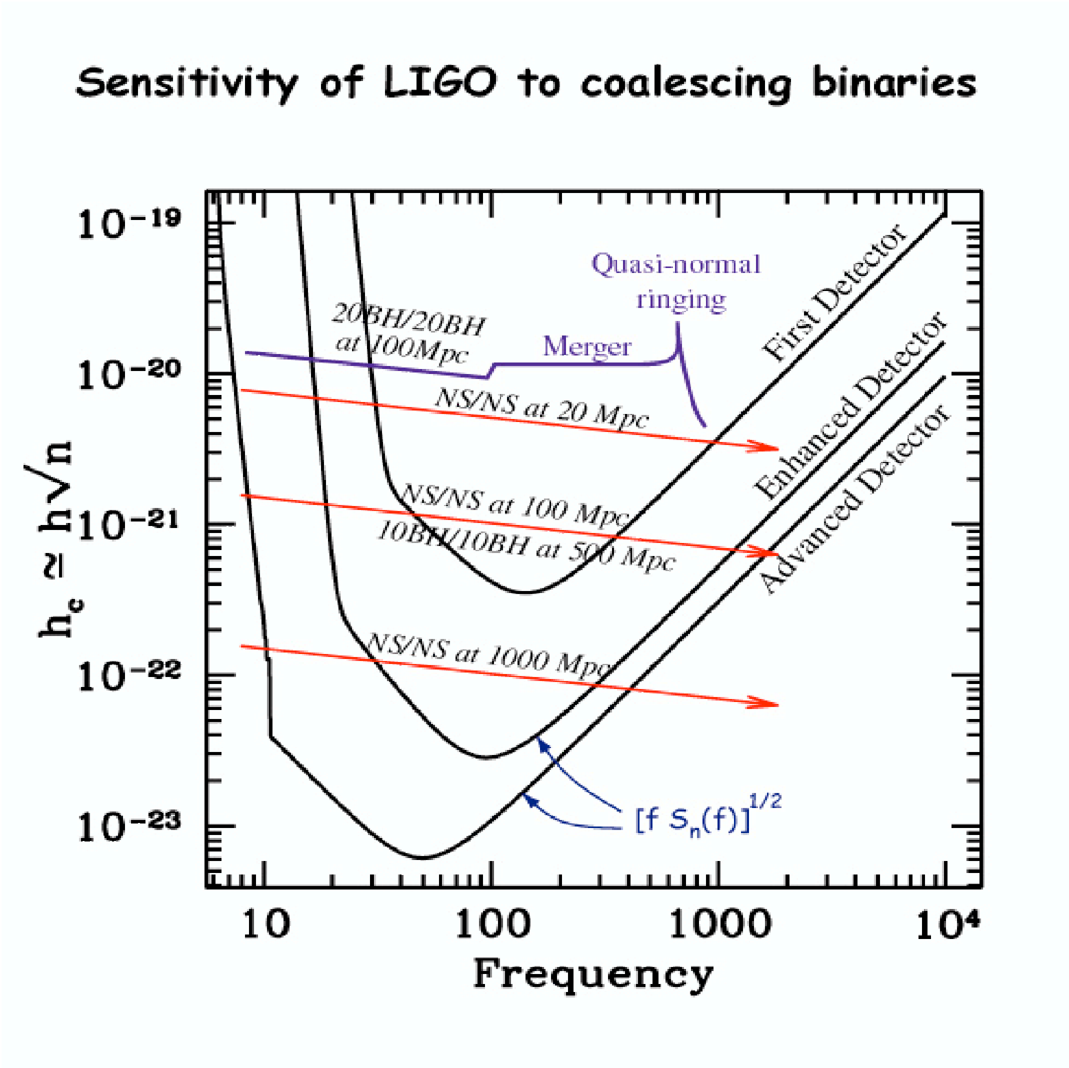

Fig. 1.6. Plot showing sensitivity curves for first and advanced generation instruments. The trajectories correspond to the power spectra for signals arising from the indicated sources.

1.2.1.3 Searches for Compact Binary Inspirals

Waveforms associated with the inspiral of $M_1+M_2 \lesssim 6M_\odot$ compact binary systems are the most well-studied sources that can be detected in the LIGO band. What is much less well known is the *rate* with which such events occur in nature. Table 1.2 presents best-estimate rates for binary systems composed of neutron star (NS) pairs, black hole (BH) pairs, and mixed systems (NS/BH) (Cutler & Thorne 2001).

The event rate for NS+NS coalescences in the Galaxy is constrained by the number of observed binary pulsars for which the energy loss due to GW emission will drive the systems to merger in a time that is shorter than $1/H_0$. The resulting constraints on the merger rate in the Galaxy, $10^{-6}\,\mathrm{yr}^{-1} \lesssim \mathcal{R}_{\mathrm{gal}} \lesssim 5 \times 10^{-4}\,\mathrm{yr}^{-1}$, extrapolates to a NS/NS event rate for the current generation of instruments that is much less than one per year. Refer to the third row of Table 1.2 for predicted event rates for initial LIGO interferometers.

Information on binary systems is inferred from observations of radio pulsars. Unfortunately, there are no known NS/BH binaries in which the NS is also a pulsar. Therefore, it is necessary to rely on much less certain estimates based on simulations of the evolution of a population of progenitor binary systems to determine the number of systems that lead to compact NS/BH binaries.

It is important to note that the uncertainties in these predicted rates span *3* orders of magnitude. However, it appears to be the case that a one-year observation with current LIGO interferometers is likely to not observe these types of events. The best direct observational limit to date, placed with data from the LIGO 40 m prototype interferometer (Allen et al. 1999), is $\mathcal{R} \leq 4400\,yr^{-1}$ (90% confidence level) for the Galaxy. S1 will provide a significantly improved observational limit.

The detection technique relies on optimal Wiener filtering in the frequency domain. The interferometer strain data are correlated with theoretically derived signal waveforms (templates), weighted by the reciprocal of the instrument noise spectral density to produce a time series of signal-to-noise ratio. The templates, $\tilde{T}(\vec{\alpha} : f)$, are characterized by a parameter vector $\vec{\alpha}$:

$$SNR(\vec{\alpha} : t) = \int_0^\infty df \frac{\tilde{h}(f)\tilde{T}^\star(\vec{\alpha} : f)}{S_n(f)} e^{-2\pi i f t}. \tag{1.1}$$

The SNR time series is processed by a thresholding algorithm to identify putative events to be further analyzed.

Figure 1.6 shows the dependence of coalescence signals on frequency. The ordinate gives the so-called "characteristic" strain of an inspiral signal. This quantity is the square root of the signal power spectral density multiplied by the number of cycles in the waveform at that frequency: it is a measure of the total power radiated at any given frequency during a coalescence event. This shows that the initial generation of LIGO interferometers can detect coalescence events for NS+NS systems to $D \approx 100$ Mpc. Also shown on the graph is the signal strength calculated for more massive $(10M_\odot + 10M_\odot)$ BH systems at distances $D \approx 500$ Mpc. For more massive systems, the merger and ringdown phases of the coalescence are detectable in the LIGO band. However, the details of the merger phase are presently unknown and require much more effort in numerical relativity simulations before templates can be provided for the data analysis. For the S1 run, systems more massive than NS+NS will not be considered. However, there is a considerable effort in the collaboration to implement template-based searches by the time of the S2 run to look for more massive systems. These searches will be predicated on analytical models that extend the waveform space beyond NS+NS systems (Buonanno, Chen, & Vallisneri 2003a,b).

1.2.1.4 Searches for a Stochastic Gravitational Wave Background

Gravitational waves of cosmological origin produce a stochastic background analogous to the relic microwave background radiation, but arising at a much earlier epoch. The search for such a signal is performed by cross-correlating the strain signals from pairs of in-

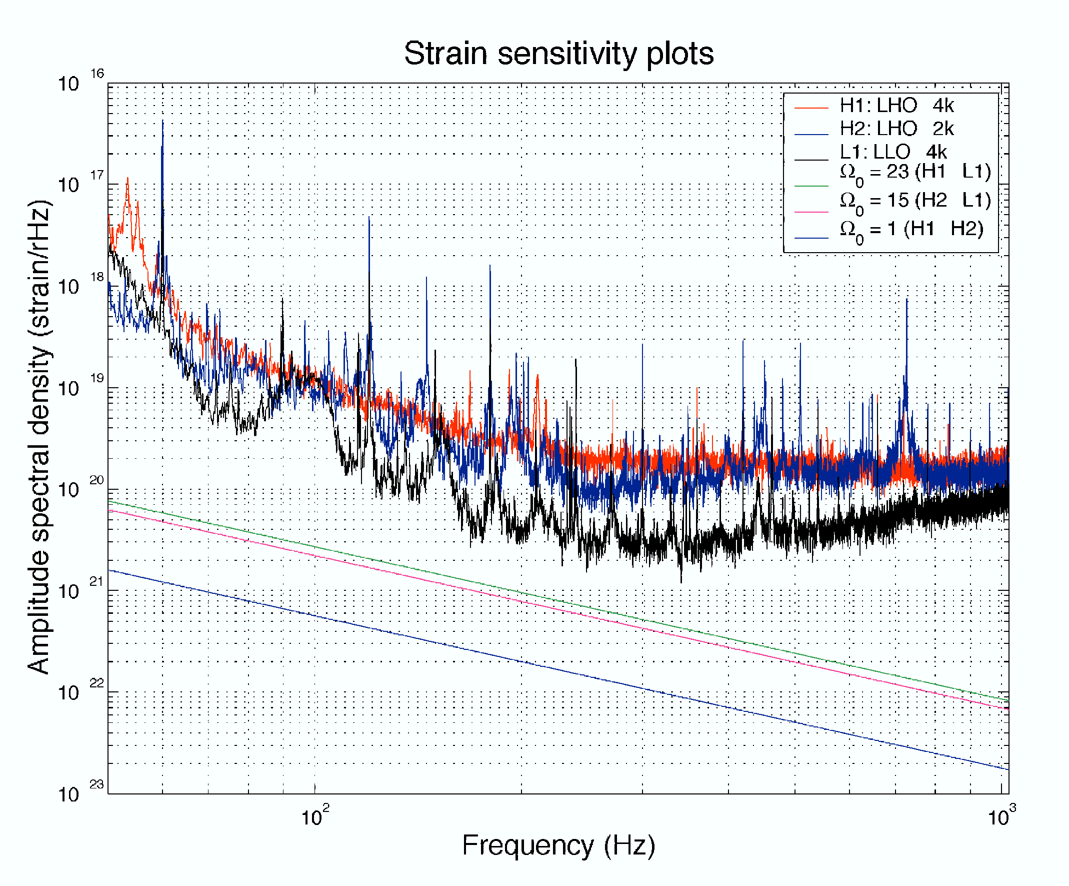

Fig. 1.7. Superposition of the S1 sensitivities of the three LIGO interferometers with predicted sensitivities of different interferometer pairs to an $\Omega_{GW}(f)$ = constant stochastic background.

terferometers and introducing an optimal Wiener filter to maximize detection signal-to-noise ratio (Michelson 1987; Christensen 1992; Flanagan 1993; Allen & Romano 1999).

The background is stochastic in the sense that its properties are only statistically characterized. Its spectral properties are described by the dimensionless quantity

$$\Omega_{\rm gw}(f) \equiv \frac{f}{\rho_{\rm critical}} \frac{d\rho_{\rm gw}}{df} , \tag{1.2}$$

where $\rho_{\rm gw}$ is the energy density in gravitational waves and

$$\rho_{\rm critical} = \frac{3c^2 H_0^2}{8\pi G} \tag{1.3}$$

is the energy density required (today) to close the Universe. H_0 is the Hubble expansion rate in the present epoch (Bennett et al. 2003):

$$H_0 \quad \equiv \quad h_{100} 100 \text{ km s}^{-1} \text{Mpc}^{-1} \approx 3.24 \times 10^{-18}\, h_{100} \text{ s}^{-1} \tag{1.4}$$

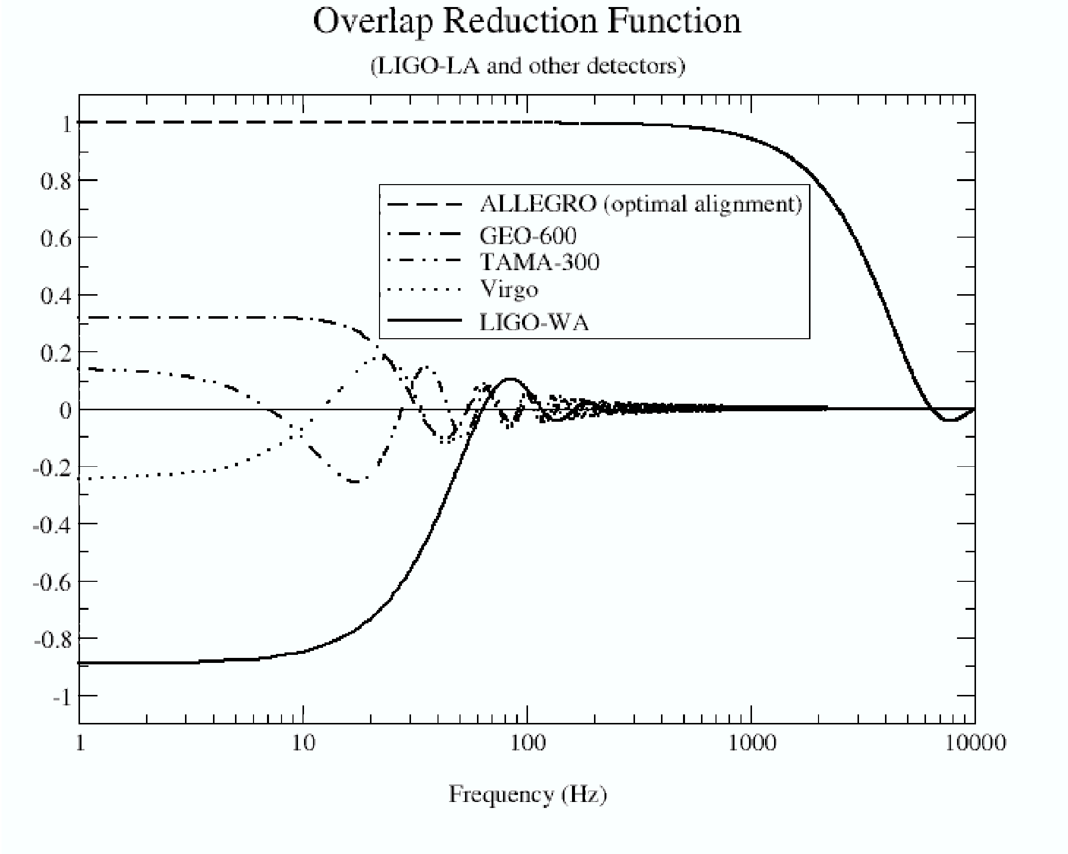

Fig. 1.8. Overlap reduction function between LIGO Livingston and the other major interferometers plus the LSU cryogenic resonant bar detector ALLEGRO (in an optimal alignment of 72° East of North).

$$= \quad 71^{+4}_{-3}\ \mathrm{km\,s^{-1}\,Mpc^{-1}} \tag{1.5}$$

Note that $\Omega_{\rm gw}(f)\, h_{100}^2$ is independent of the actual Hubble expansion rate, and has been used extensively in the literature when H_0 was not known very accurately. $\Omega_{\rm gw}(f)$ is related to the one-sided power spectral density of GW strain $S_{\rm gw}(f)$ via *

$$S_{\rm gw}(f) = \frac{3H_0^2}{10\pi^2}\, f^{-3}\Omega_{\rm gw}(f)\ . \tag{1.6}$$

Thus, for a stochastic GW background with $\Omega_{\rm gw}(f)$ = constant, the power in gravitational waves falls off as $1/f^3$.

The spectrum $\Omega_{\rm gw}(f)$ completely specifies the statistical properties of a stochastic background of gravitational radiation, provided we make several additional assumptions. Namely, we assume that the stochastic background is (1) isotropic, (2) unpolarized, (3) stationary, and

* $S_{\rm gw}(f)$ is defined by $\lim_{T\to\infty} \frac{1}{T}\int_0^T |h(t)|^2\, dt = \int_0^\infty S_{\rm gw}(f)\, df$, where $h(t)$ is the GW strain in a single detector due to the stochastic background signal.

Table 1.3. *Summary of Upper Limits on* $\Omega_0\, h_{100}^2$†

Observational Technique	Observed Limit	Frequency Domain (Hz)	Ref.‡
Cosmic Microwave Background	$\Omega_{\rm gw}(f)\, h_{100}^2 \leq 7 \times 10^{-11} \left(\frac{H_0}{f}\right)^2$	$H_0 < f < 30\, H_0$	1
Radio Pulsar Timing	$\Omega_{\rm gw}(f)\, h_{100}^2 \leq 4.8 \times 10^{-9} \left(\frac{f}{f_0}\right)^2$	$f_0 = 10^{-8}$	2
Big Bang Nucleosynthesis	$\int_{f>10^{-8}\ \rm Hz} d \ln f\ \Omega_{\rm gw}(f)\, h_{100}^2 \leq 10^{-5}$	$f > 10^{-8}$	3
Room Temp. Resonant Bar (correlation)	$\Omega_{\rm gw}(f)\, h_{100}^2 \leq 3000$	$f = 900$	4
Interferometers	$\Omega_{\rm gw}(f)\, h_{100}^2 \leq 3 \times 10^5$	$100 < f < 1000$	5
Cryogenic Resonant Bar (single)	$\Omega_{\rm gw}(f)\, h_{100}^2 \leq 300$ $\Omega_{\rm gw}(f)\, h_{100}^2 \leq 5000$	$f = 907$ $f = 1875$	6
Cryogenic Resonant Bar (correlation)	$\Omega_{\rm gw}(f)\, h_{100}^2 \leq 60$	$f = 907$	7

†The upper portion of the Table lists limits derived from astrophysical observations. The lower portion lists limits obtained from prior direct measurement. ‡References: (1) Wright et al. 1992, Bennett et al. 1996; (2) Kaspi, Taylor, & Ryba 1994; (3) Kolb & Turner 1990; (4) Hough et al. 1975; (5) Compton, Nicholson, & Schutz 1994; (6) Astone et al. 1996, 1999a; (7) Astone et al. 1999b, 2000.

(4) Gaussian. Anisotropic or non-Gaussian backgrounds [e.g., due to an incoherent superposition of GW from a large number of unresolved white dwarf binary star systems in our own Galaxy, or a "popcorn" stochastic signal produced by GW from supernova explosions (Blair & Ju 1996; Blair et al. 1997)] will require different data analysis techniques than what is being used for the S1 analysis; see, for example, Allen & Ottewill (1997) and Drasco & Flanagan (2003) for detailed discussions of these different techniques.

Cross correlating interferometer signals with an optimal Wiener filter allows one to detect the presence of a correlated signal at levels several orders of magnitude weaker than the noise spectral density. Figure 1.7 presents theoretical predictions for the magnitudes of stochastic signals arising from a Ω_{GW} = constant background that was at the limits of detectability during S1.

Under the assumptions discussed above, the optimally filtered estimate of the stochastic background is

$$\Omega_{GW}^{estimate} \approx \int_0^\infty df\, \frac{\gamma(|f|)\tilde{s}_1^\star(f)\tilde{s}_2(f)}{|f|^3 \tilde{S}_{n1}(|f|)\tilde{S}_{n2}(|f|)}, \tag{1.7}$$

where $\tilde{s}_i(f)$ are the strain signals from the interferometers and $\tilde{S}_{ni}(f)$ are their noise spectral densities. The function $\gamma(|f|)$ is a geometrical-form factor describing the frequency-dependent response of an antenna pair due to their space-time separation (Flanagan 1993). The response is for an isotropic, unpolarized irradiation by a stochastic GW background; refer to Figure 1.8, which shows $\gamma(|f|)$ for a number of interferometer pairs and also for the

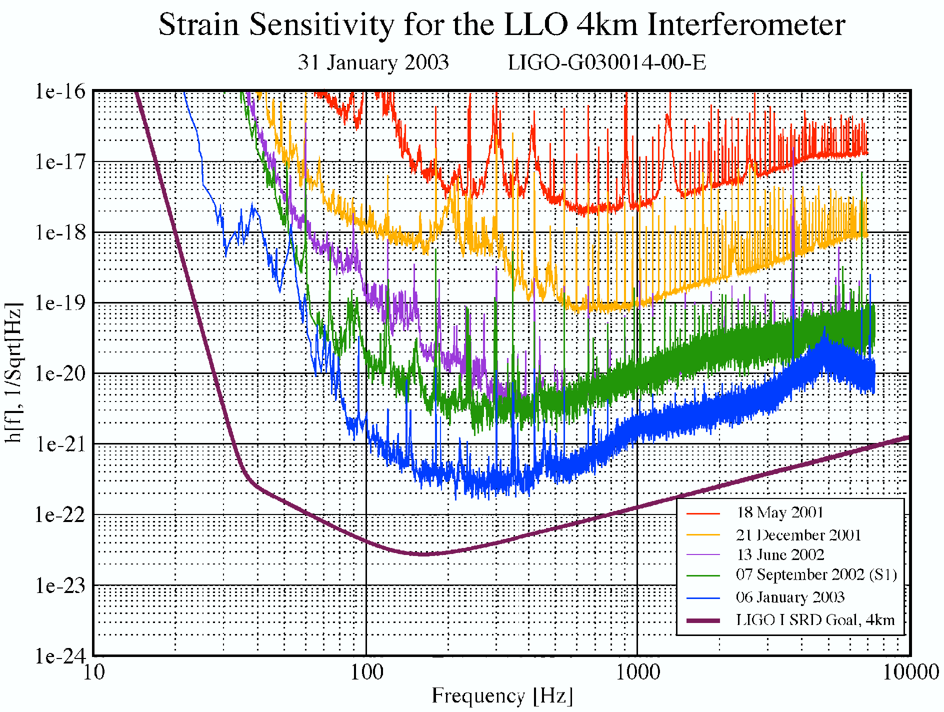

Fig. 1.9. Cascade plot of strain sensitivity improvements for the LA 4 km interferometer, showing progress in performance over the past ∼20 months. The data set] second from the bottom shows the S1 sensitivity. The bottom data set was measured about one month before the start of S2. The solid curve gives the ultimate initial LIGO design performance.

LA 4 km interferometer + ALLEGRO cryogenic bar. It is expected that the S1 run will produce a limit for Ω_{GW} that is better than previous direct determinations of this quantity in the decade frequency band 50 Hz $\lesssim f \lesssim$ 500 Hz. Table 1.3 presents a comprehensive summary of what is known or has been inferred about the stochastic GW background.

1.3 Summary

LIGO has begun scientific operation and the results for the first science run, S1, are in the process of being analyzed by the collaboration. The primary focus of the S1 run has been to develop the analysis pipelines that will be used to process the strain data for a variety of GW sources. At the same time, it is expected that the results of this analysis will achieve *direct* observational limits on the flux of gravitational radiation from these source classes, which improve on presently published limits.

At the time of this writing, a longer science run, S2, is in progress and will end in mid-April 2003. The instruments are performing ∼ 10 times *better* than they were for S1. Over the past 18 months there has been a breathtaking pace of improvement in the sensitivity of the machines (refer to Fig. 1.9). The LIGO instruments should approach their design sensitivities within a year.

1.4 Note added in proof

The preliminary results from the S1 data analysis were presented at the AAAS Symposium, *Looking Beyond Earth*, at Denver, CO in February 2003 and an update will be presented at the Spring Meeting of the APS at Philadelphia, PA in April 2003. They may be briefly summarized as follows:

- The upper limit for burst events occurring during the S1 observation was set at $\mathcal{R}_{\rm bursts} \lessapprox 2$ events day^{-1} (90% confidence level) for signals with peak strain amplitude $h \approx 4 \times 10^{-17}$ having millisecond duration. The strain sensitivity for this rate limit is ~ 5 times less stringent than has been reported by the cryogenic resonant bar consortium (IGEC).
- The search for compact binary inspirals covered the entire Milky Way galaxy, including its two satellites, the Large and Small Magellanic Clouds. This represents the first time a direct GW search extended beyond our Galaxy. The maximum range detectable for a signal-to-noise ratio = 8 event corresponded to ~ 210 kpc for the LA 4 km interferometer. The search covered the mass range for individual binary components $1M_\odot \le M_{1,2} \le 3M_\odot$. The upper limit in event rate was determined to be $\mathcal{R}_{\rm inspirals} \le 164$ events yr^{-1} per Milky Way equivalent galaxy (90% confidence level).
- The search for periodic sources targeted the millisecond EM pulsar J1939+2134 (D = 3.6 kpc). At 95% confidence using a Bayesian analysis, the maximum detectable signal from this EM source that would have been detected is $h_{CW} \le 1.4 \times 10^{-22}$.
- The search for a stochastic GW background achieved an upper limit sensitivity for the LA 4 km – WA 4 km interferometer pair, corresponding to $\Omega_{GW}(f) \le 73$ (90% confidence level) over the frequency interval 40Hz $\le f \le$ 314Hz.

Acknowledgements. The author is indebted to his colleagues within the LIGO Laboratory and the LIGO Scientific Collaboration, without whose collective participation the S1 run and the subsequent results could not have been achieved. LIGO Laboratory operates under cooperative agreement PHY-0107417. This document has been assigned the LIGO Laboratory document number LIGO-P020035-00.

References

Abramovici, A., et al. 1992, Science, 256, 325
Allen, B., et al. 1999, Phys. Rev. Lett., 83, 1498
Allen, B., & Ottewill, A. C. 1997, Phys. Rev. D, 56, 545
Allen, B., & Romano, J. D. 1999, Phys. Rev. D, 59, 102001
Anderson, W. G., Brady, P. R., Creighton, J. D., & Flanagan, É. 2000, Int. Journ. Mod. Phys. D, 9 303
——. 2001, Phys. Rev. D, 63, 042003
Andersson, N. 1998, ApJ, 502, 708
Andersson, N., Kokkotas, K., & Schutz, B. F. 1999, ApJ, 510, 846
Arras, P., Flanagan, É. É., Morsink, S. M., Schenk, A. K., Teukolsky, S. A., & Wasserman, I. 2003, ApJ, 591, 1129
Astone, P., et al. 1996, Phys. Lett. B, 385, 421
——. 2002, Phys. Rev. D, 65, 022001
——. 1999a, A&A, 343, 19
——. 1999b, A&A, 351, 811
Astone, P., Ferrari, V., Maggiore, M., & Romano, J. D. 2000, Int. Journ. Mod. Phys. D, 9, 361
Barish, B. C., & Weiss, R. 1999, Phys. Today, 52, 44 (`http://www.ligo.caltech.edu`)
Bennett, C. L., et al. 1996, ApJ, 464, L1

——. 2003, ApJS, 148, 1
Bildsten, L., & Ushomirsky, G. 2000, ApJ, 529, L33
Blair, D., Burman, R., Ju, L., Woodings, S., Mulder, M., & Zadnik, M. G. 1997, preprint
Blair, D., & Ju, L. 1996, MNRAS, 283, 648
Brady., P. R., & Creighton, T. 2000, Phys. Rev. D, 61, 082001
Brady., P. R., Creighton, T., Cutler, C., & Schutz, B. F. 1998, Phys. Rev. D, 57, 2101
Buonanno, A., Chen, Y., & Vallisneri, M. 2003a, Phys. Rev. D, 67, 104025
——. 2003b, Phys. Rev. D, 67, 024016
Caron, B.. et al. 1995, in First Edoardo Amaldi Conference on Gravitational Wave Experiments, ed. E. Coccia, G. Pizzella, & F. Ronga (Singapore: World Scientific), 86
Christensen, N. 1992, Phys. Rev. D, 46, 5250
Compton, K., Nicholson, D., & Schutz, B. F. 1994, Proceedings of the Seventh Marcel Grossman Meeting on General Relativity, ed. R. T. Jantzen, G. M. Keiser, & R. Ruffini (River Edge, New Jersey: World Scientific), 1078
Cutler, C., & Thorne, K. 2001, in Proceedings of GR16, Durban, South Africa
Danzmann, K., et al. 1995, in First Edoardo Amaldi Conference on Gravitational Wave Experiments, ed. E. Coccia, G. Pizzella, & F. Ronga (Singapore: World Scientific), 100
Drasco, S., & Flanagan, É. É. 2002, in Proceedings of the Ninth Marcel Grossmann Meeting on General Relativity, ed. V. G. Gurzadyan, R. T. Jantzen, & R. Ruffini (River Edge, New Jersey: World Scientific), in press
Ferrari, V. 1997, in Proceedings of the 12th Italian Conference on General Relativity and Gravitational Physics, ed. M. Bassan et al. (Singapore: World Scientific), 149
Finn, L. S., Mohanty, S. D., & Romano, J. D. 1999, Phys. Rev. D, 60, 121101
Flanagan, É. É. 1993, Phys. Rev. D, 48, 2389
Friedman, J. L., & Morsink, S. M. 1998, ApJ, 502, 714
Hough, J., Pugh, J. R., Bland, R., & Drever, R. W. P. 1975, Nature, 254, 498
Hough, J., Ward, H., Munley, A. J., Newton, G. P., Meers, B. J., Hoggan, S., Kerr, G. A., & Drever, R. W. P. 1983, Nature, 303, 216
Jones, P. B. 2001, Phys. Rev. D, 64, 084003
Kaspi, V. M., Taylor, J. H., & Ryba, M. F. 1994, ApJ, 428, 713
Kolb, E. W., & Turner, M. S. 1990, in The Early Universe (Reading, MA: Addison Wesley)
Lindblom, L., & Owen, B. J. 2002, Phys. Rev. D, 65, 063006
Lindblom, L., Owen, B. J., & Morsink, S. M. 1998, Phys. Rev. Lett., 80, 4843
Michelson, P. F. 1987, MNRAS, 227, 933
Pradier, T., Arnaud, N., Bizouard, M.-A., Cavalier, F., Davier, M., & Hello, P. 2001, Phys. Rev. D, 63, 042002
Sylvestre, J. 2002, Phys. Rev. D, 66, 102004
Tsubono, K. 1995, in First Edoardo Amaldi Conference on Gravitational Wave Experiments, ed. E. Coccia, G. Pizzella, & F. Ronga (Singapore: World Scientific), 112
Wright, E. L., et al. 1992, ApJ, 396, L13
Zwerger, T., & Müller, E. 1997, A&A, 320, 209